ISSN: 2277-3754
ISO 9001:2008 Certified
International Journal of Engineering and Innovative Technology (IJEIT)
Volume 8, Issue 4, October 2018

Properties Characterization of Functional Graded High Heat Resistance Materials via Meshless Radial Point Interpolation

Hsin-Yi Lai [1] and Jing-Hao Kang[2]
Department of Mechanical Engineering, National Cheng-Kung University, Tainan, Taiwan, R.O.C. [1,2]

Abstract*—In this article, a Meshless Radial Point Interpolation (MRPI) method is applied to characterize thermo elastic and fracture properties of functional graded high heat resistance materials. As compared to the Finite Element Method (FEM), the proposed meshless method is much easier in dealing with complicated boundaries including crack and large deformation at edges. In the formulation a weak form is adopted to establish system governing equations and MRPI is applied to discrete the problem domain. From the results of simulation for stress intensity factor (SIF) calculation, the estimation by using MRPI is found more precise than those obtained by FEM approaches. As compared to the analytical solution for homogeneous cracked plates bearing tension stress and heat flows, the estimation error obtained by MRPI is approximately 1.15%, and -22.5% for FEM approach. The influence of different volume fraction of FGMs that bear time-dependent external force and temperature variation at different crack locations for various crack lengths are also investigated and documented. The results are found satisfactorily accurate and thus can be used to predict fracture characters of inhomogeneous and functional graded materials for engineering design applications.

***Index Terms*—Meshless, MFree RPIM, Stress Intensity Factor, Functionally Graded Materials.**

I. INTRODUCTION

In the past, composite plates were widely used in industry to strengthen the intensity of the structure [1]. However, many inherent discontinuous interfaces of composite plates are likely to cause stress concentration and to largely reduce the reliability and strength of materials. With recent advancement in high technology, functionally graded materials (FGMs) have been gradually emerged as a replacement for composite structural elements [2-4]. The concept of FGMs was also proposed to deal with thermal barriers problems in aerospace industry recently. Among them, many different types of FGMs were used in high working temperature environment, including thermal shock or being heated/cooled in short term. Since FGMs can also be made by using two or more individual constituents to enhance mechanical properties via grading volume fraction of constituents, varying from 0% to 100%, it can be used to combine metal and ceramic into the FGMs [5, 6]. By so doing, FGMs possess the advantages of both structural flexibility of metal and heat resistance of ceramic. However, the FGMs are inevitable existing some defects including vacancies and cracks inside the structures [7-9] and since it's very difficult to obtain analytical solutions for such inhomogeneous materials with cracks subjected to complex boundary conditions [10-13]. A mesh free method is thus introduced to characterize thermal and dynamic behaviors of such FGMs with cracks.

Meshfree methods have been developed for solving complex boundary engineering problems over past two decades. There are several different computational schemes for mesh free, such as smooth particle hydrodynamics (SPH), diffuse element method (DEM), element free Galerkin method (EFGM), mesh free local Petrov-Galerkin method (MLPG), point interpolation method (PIM) and radial point interpolation method (MRPI). The main concept of mesh free method is to establish a system of algebraic governing equations without using a predefined mesh for domain discretization. Meshfree methods employ arbitrary and scattered nodes that have no relationship between them to discretize governing equations. There are several methods that have been applied for structural analysis in the past. In this study, MRPI is selected as our major computational scheme mainly for its simplicity. The MRPI we developed here is one of the well-known meshfree schemes [14] using the radial basis function as approximation functions. Since radial basis functions satisfy Kronecker's delta properties, it's easy to enforce the associated essential boundary conditions by including direct method and penalty functions.

This paper is mainly to employ the aforementioned computational scheme to characterize thermo elastic and fracture properties of FGM plates with crack subjected to thermal and mode-I loadings. The influence of stress and displacement as expressed in terms of crack locations and volume fractions of FGMs are fully explored.

II. METHOD

A. *Meshless Radial Point Interpolation Method (RPIM)*

The radial basis function (RBF) is first used to develop the radial point interpolation shape functions for the meshfree weak-form. To avoid singularity problem the radial basis function is thus added. The MRPI interpolation can be written as

$$u(\mathrm{x}) = \sum_{i=1}^{n} R_i(\mathrm{x})\,\mathrm{a}_i + \sum_{j=1}^{m} p_j(\mathrm{x})\,\mathrm{b}_j = R^T(\mathrm{x})\,\mathrm{a} + p^T(\mathrm{x})\,\mathrm{b} \qquad (1)$$

ISSN: 2277-3754
ISO 9001:2008 Certified
International Journal of Engineering and Innovative Technology (IJEIT)
Volume 8, Issue 4, October 2018

Where R(x) is the radial basis function, is the monomial in x, y coordinates, and n is the number of radial basis functions. In R(x), the variable is of the distance between x, the point of interest, and the node of xi, such that

$$r = \sqrt{(\mathrm{x}-\mathrm{x}_i)^2 + (\mathrm{y}-\mathrm{y}_i)^2} \tag{2}$$

There are many types of radial basis functions in which the characteristics of RBFs are widely discussed, including multi-quadrics, Gaussian or exponential, thin plate spline and logarithmic, etc. In this work, a multi-quadrics (MQ) scheme is used to develop the MQ shape function that is given as

$$R_i(x,y) = \left(r_i^2 + (\alpha_c d_c)^2\right)^q \tag{3}$$

In the above equation, three unknown parameters of ac , dc and q are to be determined, where ac and q can be determined by a given designated performance, and dc is the characteristic length, which can be chosen as the average distance between nodes in the domain. To solve the unknown coefficients of vectors a and b in Eq. (1), one must enforce the equation to be satisfied at the n given nodes surrounding the point of interest x. This leads to a set of n equations that can be expressed as

$$U_s = R_0 a + P_m b \tag{4}$$

Here, the vector function is given as

$$U_s = \{u_1 \quad u_2 \quad \cdots \quad u_n\}^T \tag{5}$$

and the moment matrix of RBFs is presented as

$$R_0 = \begin{bmatrix} R_1(r_1) & R_2(r_1) & \dots & R_n(r_1) \\ R_1(r_2) & R_2(r_2) & \dots & R_n(r_2) \\ \vdots & \vdots & \ddots & \vdots \\ R_1(r_n) & R_2(r_n) & \dots & R_n(r_n) \end{bmatrix} \tag{6}$$

Where r_k is defined by

$$r_k = \sqrt{(x_k - x_i)^2 + (y_k - y_i)^2} \tag{7}$$

The polynomial moment matrix turns out to be as

$$U_s = \{u_1 \quad u_2 \quad \cdots \quad u_n\}^T \tag{8}$$

Since there are *n*+*m* variables in Eq. (8), it is required to add another m equations in order to solve the problem. Therefore, we further assume that

$$P_m^T a = \sum_{i=1}^{n} p_j(x_i) a_i = 0 \tag{9}$$

By applying Eq. (9) to Eq. (4), one can obtain

$$\tilde{U}_s = \begin{bmatrix} U_s \\ 0 \end{bmatrix} = \begin{bmatrix} R_0 & P_m \\ P_m^T & 0 \end{bmatrix} \begin{Bmatrix} a \\ b \end{Bmatrix} = G a_0 \tag{10}$$

Since matrix R_0 is symmetric, the matrix of *G* will also be symmetric. By solving the inverse form of Eq. (10), one can easily obtain

$$a_0 = \begin{Bmatrix} a \\ b \end{Bmatrix} = G^{-1} \tilde{U}_s \tag{11}$$

After plugging Eq. (11) into Eq. (1), the result can be obtained as

$$u(\mathrm{x}) = \mathrm{R}^T(\mathrm{x})\,\mathrm{a} + \mathrm{p}^T(\mathrm{x})\,\mathrm{b} = \left\{R^T(\mathrm{x}) \;\; \mathrm{p}^T(\mathrm{x})\right\} G^{-1} \tilde{U}_s \tag{12}$$

Finally, the solution can be rearranged into the form as

$$u(x) = \left\{R^T(x) \;\; p^T(x)\right\} G^{-1} = \tilde{\Phi}^T(x) \tilde{U}_s \tag{13}$$

Where $\tilde{\Phi}^T(x)$ is the shape function, and

$$\tilde{\Phi}^T(x) = \{\phi_1(x) \quad \phi_2(x) \quad \dots \quad \phi_n(x) \quad \phi_{n+1}(x) \quad \dots \quad \phi_{n+m}(x)\}$$

B. *Formulation of Global Galerkin Weak-form*

As we know, the Global Galerkin weak-form can be derived by using Galerkin weighted residual method, virtual work principle and the principle of minimum potential energy. Consider a system governed by the differential equations in the problem domain Ω as

$$A(u) + b = 0 \tag{14}$$

Where *A* is a differential operator dealing with the scalar function u. And the boundary condition is given as on the boundary Γ as

$$C(u) = d \tag{15}$$

Where *C* is a differential operator associated with the boundary condition. Assume that a system of governing equations are expressed in terms of ODEs or PDEs, and are to be solved for approximate solutions. The function u can be approximated as

$$u^p = \sum_{i=1}^{n} \alpha_i B_i(x) \tag{16}$$

Where $B_i(x)$ the basis functions, a_i are unknown coefficients, and *n* is the number of basis functions. By plugging Equation (16) into Equations (14) and (15), the following equations can be obtained as

$$A(u^p) + b \neq 0 \tag{17}$$

$$C(u^p) - d \neq 0 \tag{18}$$

Here, the residual functions of R_A and R_C can be thus derived, respectively, as

$$R_A = A(u^p) + b \tag{19}$$

$$R_C = C(u^p) - d \tag{20}$$

Since the residual functions of R_A and R_C always change along with the approximate functions one select to use, it is thus required for the overall domain residues to be minimized. The weighted integrals of residual functions is thus enforced to be zero in the process and that can be expressed as

$$\int_{\Omega} W_i R_A d\Omega + \int_{\Gamma} Q_i R_C d\Gamma = 0 \tag{21}$$

Where W_i and Q_i are the weighted functions of R_A and R_C. Eq. (21) is the general form of the weighted residual approach. They are a set of integral equations that is derived from the original system ODEs or PDEs

C. *Basic Assumptions and Modeling Procedures*

Here the material properties are assumed to be varied along *x* and *y* directions only, and that means the properties do not

ISSN: 2277-3754
ISO 9001:2008 Certified
International Journal of Engineering and Innovative Technology (IJEIT)
Volume 8, Issue 4, October 2018

vary along *z*-direction. Therefore, a 2D plate problem on *xy* plane is thus considered.

D. Formulations of Meshless Elastic Dynamics

Consider a two-dimensional elastic problem with a working domain of Ω and boundary of Γ, subject to a body force *b*. The governing equation can be expressed as

$$L^T\sigma + b = \rho\ddot{u} + c\dot{u} \tag{22}$$

Where ρ is the density, *c* is damping coefficient, and *u* is the displacement vector. The system differential operator *L* can thus be expressed as

$$L = \begin{Bmatrix} \frac{\partial}{\partial x} & 0 \\ 0 & \frac{\partial}{\partial y} \\ \frac{\partial}{\partial y} & \frac{\partial}{\partial x} \end{Bmatrix} \tag{23}$$

Here, boundary conditions are given as

$$\sigma \cdot n = \bar{t} \quad \text{on the natural boundary} \tag{24}$$

$$u = \bar{u} \quad \text{on the essential boundary} \tag{25}$$

Where traction $\bar{t}$ and displacement $\bar{u}$ are assumed to be known values. The weak form of Eq. (22) can then be expressed as

$$\int_\Omega (L\delta u)^T (DLu)d\Omega - \int_\Omega \delta u^T b d\Omega - \int_\Gamma \delta u^T (\rho\ddot{u} + c\dot{u})d\Omega \tag{26}$$

Where *D* is stiffness matrix. In order to obtain an approximate solution to the system, the following approximate functions are applied.

$$\delta u = \sum_I^N \phi_I \delta u_I \tag{27}$$

$$L\delta u = \sum_I^N B_I \delta u_I \tag{28}$$

$$Lu = \begin{bmatrix} \frac{\partial \phi_1}{\partial x} & 0 & \cdots & \frac{\partial \phi_n}{\partial x} & 0 \\ 0 & \frac{\partial \phi_1}{\partial y} & \cdots & 0 & \frac{\partial \phi_n}{\partial y} \\ \frac{\partial \phi_1}{\partial y} & \frac{\partial \phi_1}{\partial x} & \cdots & \frac{\partial \phi_n}{\partial y} & \frac{\partial \phi_n}{\partial x} \end{bmatrix} \begin{Bmatrix} u_1 \\ v_1 \\ \vdots \\ u_n \\ v_n \end{Bmatrix} = \sum_I^n B_I u_I \tag{29}$$

Where ϕ_i is the *i*-th shape function for the working domain? By plugging Equations (27) – (29) into Equation (26), one can obtain

$$\int_\Omega (L\delta u)^T (DLu)d\Omega = \int_\Omega \sum_I^N \sum_J^N \delta u_I [B_I^T D B_J] u_J d\Omega \tag{30}$$

$$B = \begin{bmatrix} \frac{\partial \Phi_i}{\partial x} & 0 & \frac{\partial \Phi_i}{\partial y} \\ 0 & \frac{\partial \Phi_i}{\partial y} & \frac{\partial \Phi_i}{\partial x} \end{bmatrix}^T \tag{31}$$

The governing equations can then be converted into a discrete system equations of $M\ddot{U} + C\dot{U} + KU = F^b + F^i$, where the mass matrix is given as

$$M_{IJ} = \int_\Omega \rho \phi_I^T \phi_J^T d\Omega \tag{32}$$

The stiffness matrix is represented as

$$K_{IJ} = \int_\Omega [B_I^T D B_J] d\Omega \tag{33}$$

The damping matrix is expressed as

$$C_{IJ} = \int_\Omega c \phi_I^T \phi_J^T d\Omega \tag{34}$$

And the force matrices are given as

$$F_I^b = \int_\Gamma \phi_I^T b d\Gamma \tag{35}$$

$$F_I^t = \int_\Gamma \phi_I^T \bar{t} d\Gamma \tag{36}$$

E. Formulations of Meshless Transient Heat Conduction

Consider a two-dimensional transient heat conduction problem with domain Ω and boundary Γ, the governing equation of heat conduction can be expressed as

$$\rho c \frac{\partial T(x,y,t)}{\partial t} = \frac{\partial}{\partial x}(k_x \frac{\partial T(x,y,t)}{\partial x}) + \frac{\partial}{\partial y}(k_y \frac{\partial T(x,y,t)}{\partial y}) + Q \tag{37}$$

where ρ is the density of the underlying materials, *c* is the specific heat, $T(x,y,t)$ is temperature field, k_x and k_y are the thermal conductivity coefficients in x and y directions, and *Q* is the heat generated per unit volume. Also, boundary conditions are given as

$$T = \bar{T} \quad \text{on the essential boundary} \tag{38}$$

$$-k(\nabla T \cdot n) = \bar{q} \quad \text{on the natural boundary} \tag{39}$$

$$-k\nabla T \cdot n = h(T - T_\infty) \quad \text{on the natural boundary} \tag{40}$$

$$T(x,y,0) = T_0(x,y,0) \quad \text{is the initial condition} \tag{41}$$

where $\bar{q}$ is the heat flux, T_∞ is the environment temperature, $\bar{T}$ and $T_0(x,y,0)$ are of prescribed values.

Following the same procedure as we did for elastic dynamic problems, the approximate solution for the temperature field can be given as

$$T^h(x,y,t) = \sum_{i=1}^N \phi_i^T(x,y) T(x,y,t) \tag{42}$$

By using the weak form of Eq. (40), one can derive the general form of governing equation as

$$C\dot{T} + KT = F(T,t) \tag{43}$$

where

$$C_{ij} = \int_\Omega \rho c \phi_i \phi_j d\Omega \tag{44}$$

$$K_{ij} = \int_\Omega k_x \left[\frac{\partial \phi_i}{\partial x}\frac{\partial \phi_j}{\partial x}\right] + k_y \left[\frac{\partial \phi_i}{\partial y}\frac{\partial \phi_j}{\partial y}\right] d\Omega + \int_{\Gamma_1} h\phi_i\phi_j d\Gamma \tag{45}$$

$$F_i = \int_\Omega Q\phi_i d\Omega - \int_{\Gamma_1} \bar{q}\phi_i d\Gamma - \int_{\Gamma_1} hT_\infty \phi_i d\Gamma \tag{46}$$

ISSN: 2277-3754
ISO 9001:2008 Certified
International Journal of Engineering and Innovative Technology (IJEIT)
Volume 8, Issue 4, October 2018

III. RESULTS

A. FGM Plate with Crack subjected to External Force

Since the distinct properties of FGMs, it can be applied to some extreme working environment. For example, the aerospace structures of shuttle buses can encounter vibration and high temperature in fields. Thus, SiC and steel are used in our compositions here for testing purpose. Based on the assumptions we made in Table 1, our working problem can be simplified as a plate. In the first case, we assume the loading sources coming from environment, and there are two types of loading, one being the constant force, and the other one being sine-waved force that varies with time. Our schematic diagrams are given in Figures 3 and 4. Then we investigate the relation of E2, i.e. the properties of top side materials and crack location. When the crack is located on the SiC side, i.e. E2 is the properties of SiC, and E1 is the properties of steel. Otherwise, the crack is located on the steel side, i.e. E2 is the properties of steel, and E1 is the properties of SiC. The properties of these two materials are given as

Steel： 205 GPa、$\nu = 0.3$、220 GPa、151.85 GPa。

SiC ： 410 GPa、$\nu = 0.17$、 76 GPa、 26 GPa。

Where K is bulk modulus, and is shear modulus. In this testing case, the influence of crack location and different loading types one the stress are investigated and the results are given in Fig. 5. The results indicate that the stress as expressed in terms of crack lengths and crack locations for uniform external loadings. Here, the legend of t.e. stands for the crack located on the SiC side, otherwise, b.e. stands for the crack located on the steel side. Figure 6 shows the stress as expressed in terms of crack lengths and crack locations subject to sine-waved loadings. Figure 7 shows the stress expressed in terms of crack lengths and two different loading types as the crack is located on the SiC side. And finally Figure 8 shows the stress as expressed in terms of crack lengths and two different loading types as the crack is located on the steel side.

From simulation results, one can easily observed that as the crack lies on the stronger side of SiC, the impact of volume fraction on stress is decreased as the length of crack increases. However, as the crack lies on the weaker side, the opposite result will be obtained. As far as the influence of external types of loadings on the stress development is concerned, it is observed that for two different types of loadings, one is of uniform loadings, and the other is of sine-waved loadings, the maximum values of the two type of loadings are almost the same, although the one of sine-waved loadings is somewhat smaller in both displacements and stresses during the exertion period of time.

B. FGM Plate with Crack Subjected to External Force and Heat Conduction

From the results of modeling, it is found that the properties of FGMs change directly the dynamic behaviors. So, the influences of temperature to dynamic behaviors under force vibration are investigated. Material compositions are chosen based on working environment. In this study, SiC and steel are selected as our main materials. SiC is used to contact high temperature, and steel is used to connect the structure bearing loadings. So here, the same external temperature/loading conditions and also exchanging both sides of the top and bottom base materials were arranged to explore the results for better comparisons. Figures 9 and 10 show the schematic diagrams of the FGM plate with fixed temperature at 50 degree of Celsius along all edges. The inner hole is assumed fixed that means it cannot be moved or deformed. Also, two types of loadings were applied at the bottom side. Top side is of traction free. One loading is of $F=A$ MPa, and the other one is of $F=A*sin(wt)$ Mpa. For convenience, the frequency is set to be w =1, and A=1000. In this study, we concentrate on the response of node (-12, 5.5 cm), Figure 11 shows the displacement as expressed in terms of different p values and crack location under the loadings of sin-wave. Figure 12 shows the displacement as expressed in terms of different p values and crack locations under normal uniform loading. From the results of these two figures, one can observe that the peak of displacement is smaller for the loadings of sin-wave as compared to that of the normal uniform loading. Secondly, as p=1, the properties of materials vary at the same gradient tendency. Thus, the larger the displacement as the crack is located on the SiC side. Figure 13 shows the displacement as expressed in terms of different volume fractions and loading types as crack is located on the SiC side. From Figures 11 and 12, it is found that under the situation that the direction of loadings is parallel to properties gradient, and as the crack is located on the SiC side, the bigger p value or less percentage of SiC, the larger displacement is introduced. Also, the displacement as expressed in terms of different volume fractions and loading types for the crack located on the steel side, the bigger p value, the smaller displacement is introduced. In Figures 13 and 14, the same conclusions can be also drawn.

IV. CONCLUSION

Since it is often difficult to obtain analytical solutions for inhomogeneous structures with complicated boundary conditions, numerical methods are then developed to obtain approximate solutions instead. This work is thus to introduce meshless MRPI approach to possibly characterize thermo elastic and fracture properties of FGM plates. Once the theory and computational procedures are established, several numerical studies are presented. Many geometric and material variations are also investigated and presented. Here are some conclusions and summaries.

1. In this work, meshless MRPI is introduced to characterize the thermo elastic and fracture properties of FGMs plate with different cracks and load conditions. In dealing with crack problem, this work as compared to analytical solutions, 1.15% error is obtained by using the MRPI and -22.5% by FEM modeling.
2. The influence of volume fraction and crack properties to mechanical behaviors of the FGM are characterized for cracks located at SiC side, the impact of volume fraction on stress decreases as the length of crack increases.

ISSN: 2277-3754
ISO 9001:2008 Certified
International Journal of Engineering and Innovative Technology (IJEIT)
Volume 8, Issue 4, October 2018

However, if the crack lies in the steel side, the result is opposite. For investigation of FGM heat conduction problem, it is found that on the rising percentage of SiC the value of thermal conductivity is reduced, thermal specific heat is lower as well. As a result, it achieves steady state much faster than that of the lower percentage one. In the results of FGM vibration case, no matter where the crack is located, larger displacement is obtained as the percentage of SiC decrease.

3. In conclusion, it is found that SiC does possess excellent thermal and mechanical properties. However, SIC materials is brittle, if there exists any crack, it's prone to extend quickly. Thus, the percentage of each material must be compromised in accordance with the working environment. The procedures and illustrations in this study provide a means to predict fracture behaviors and to supply information of working capability for design life liability of the structures made of FGMs.

Table 1 Dimensions and properties of the plate

Scale	L=24 mm W=12 (mm)
Density	7850 kg/m^3
Young's modulus	200 GPa
Poisson ratio	0.3
Crack length	6 mm
Stress σ	1000 MPa

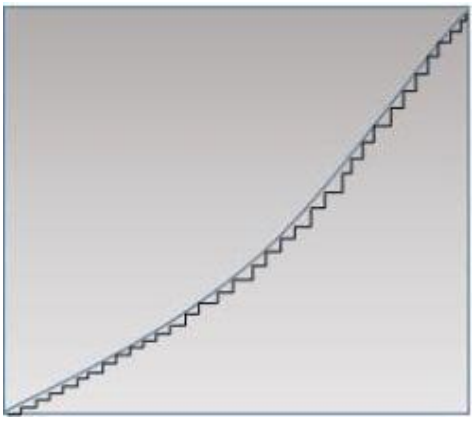

Fig. 1 Standard 3-D model (top ceramic, bottom metal)

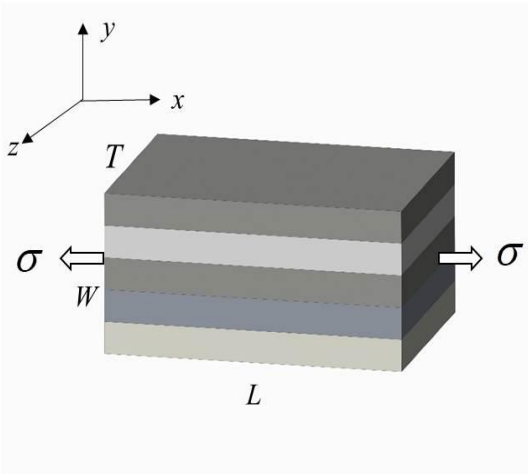

Fig. 2 Schematic diagram for functional graded materials

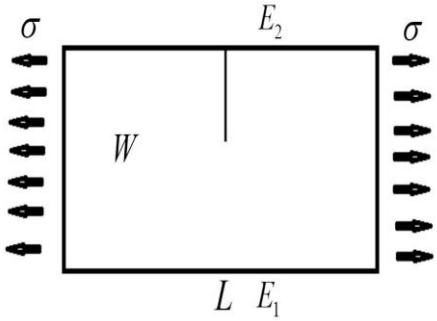

Fig. 3 Schematic diagram for functional graded materials

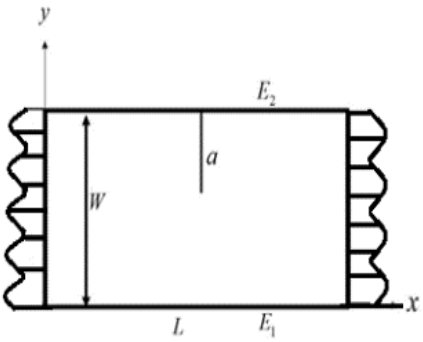

Fig. 4 diagram for sine-waved loadings, *A*=1000, *w*=1

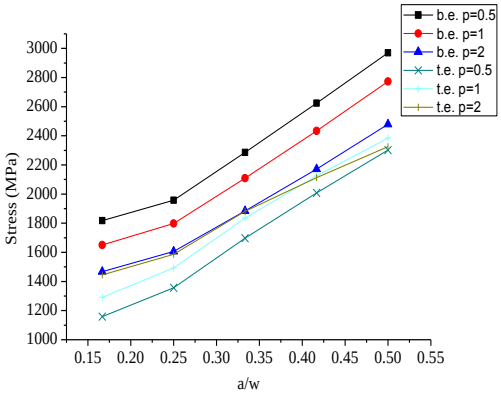

Fig. 5 Stresses for different crack lengths and locations under uniform loadings

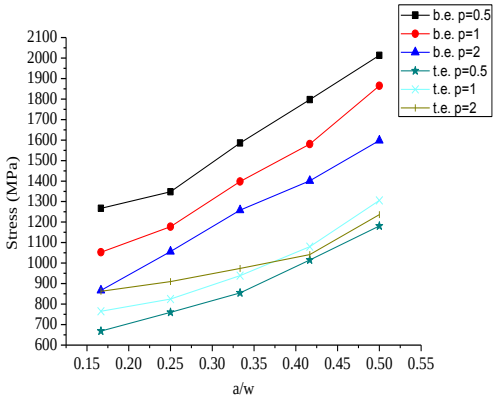

Fig. 6 Stresses for various crack lengths and locations under sin-waved force

ISSN: 2277-3754
ISO 9001:2008 Certified
International Journal of Engineering and Innovative Technology (IJEIT)
Volume 8, Issue 4, October 2018

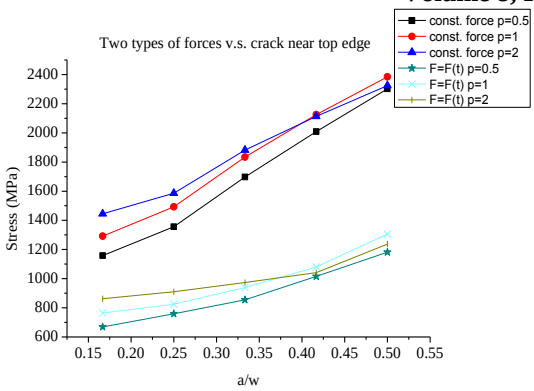

Fig. 7 Stresses for different loading types and p values as the crack is on the SiC side

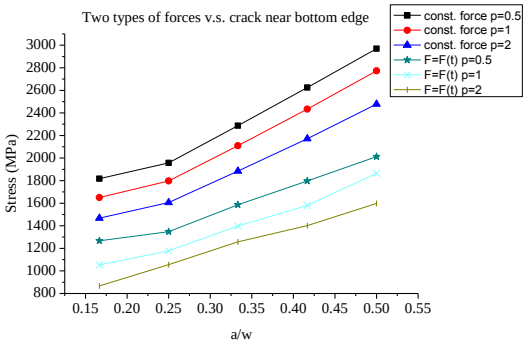

Fig. 8 Stresses for different loading types and p values as the crack is on the steel side

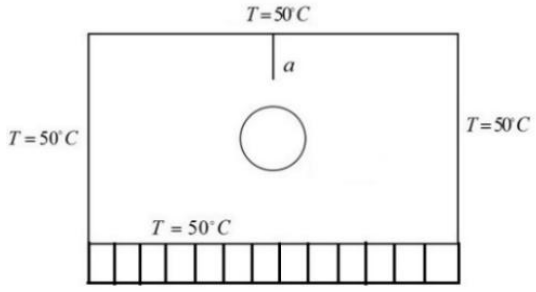

Fig. 10 Schematic diagram for uniform loadings, A=1000 MPa

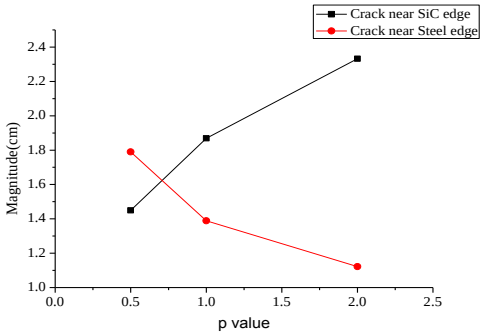

Fig. 11 Displacements for different p values and crack locations under sin-waved loadings

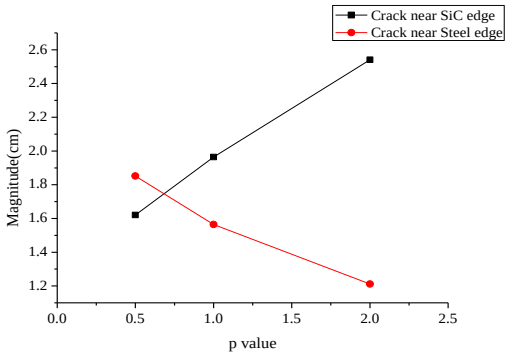

Fig. 12 Displacements for different p values and crack location under normal loadings

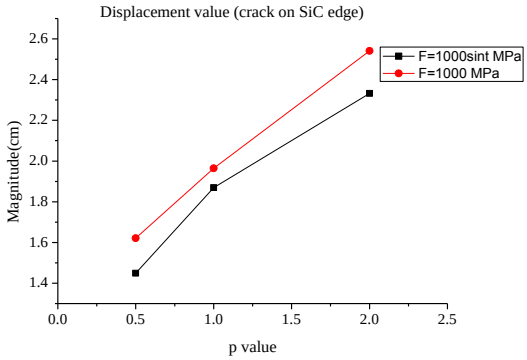

Fig. 13 Displacements for different volume fractions and loading types as the crack is located on the SiC side

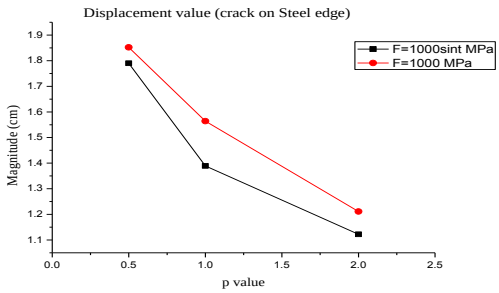

Fig. 14 Displacements for different volume fractions and loading types as the crack is located on the steel side

REFERENCES

[1] H. Hatta and M. Taya, "Effective Thermal Conductivity of a Misoriented Short Fiber Composite," J. Appl. Phys., vol. 58, no. 7, pp. 2478-2486, 1986.

[2] B. Kieback, A. Neubrand, and H. Riedel, "Processing Techniques for Functionally Graded Materials," Materials Science and Engineering, A362, pp. 81-105, 2003.

[3] A.J. Markworth, K.S. Ramesh, and W.P. Parks, "Review: Modeling Studies Applied to Functionally Graded Materials," J. Mater. Sci., vol. 30, pp. 2183-2193, 1995.

[4] Y. Miyamoto, W.A. Kaysser, B.H. Rabin, A. Kawasaki, R.G. Ford, Functionally Graded Materials: Design, Processing and Applications, Kluwer Academic, Dordrecht, 1999.

ISSN: 2277-3754
ISO 9001:2008 Certified
International Journal of Engineering and Innovative Technology (IJEIT)
Volume 8, Issue 4, October 2018

[5] T. Mori, K. Tanaka," Average Stress in Matrix and Average Elastic Energy of Materials with Misfitting Inclusions," Acta Metallurgica, vol. 21, pp. 571-574, 1973.

[6] N. Noda, "Thermal Stresses in Functionally Graded Materials," J. Therm. Stresses, vol. 22, pp. 477-512, 1999.

[7] G.H. Paulino, Z.H. Jin, and R.H. Dodds, "Failure of Functionally Graded Materials," Compreh. Structural Integrity, Elsevier Science, New York, vol. 2, pp. 607-644, 2003.

[8] M.-J. Pindera, S.M. Arnold, J. Aboudi, and D. Hui, "Use of Composites in Functionally Graded Materials," Composites Eng., vol. **4**, pp. 1-145, 1994.

[9] M.-J. Pindera, J. Aboudi, A.M. Glaeser, and S.M. Arnold, "Use of Composites in Multi-Phased and Functionally Graded Materials," Composites, B28, pp. 1-175, 1997.

[10] B.W. Rosen and Z. Hashin, "Effective Thermal Expansion Coefficients and Specific Heats of Composite Materials," Int. J. Eng. Sci., vol. 8, pp. 157-173, 1970.

[11] S. Suresh and A. Mortensen, Fundamentals of Functionally Graded Materials, IOM Communications, London, 1998.

[12] K. Tanaka, Y. Tanaka, K. Enomoto, V.F. Poterasu, Y. Sugano, "Design of Thermo elastic Materials using Direct Sensitivity and Optimization Methods. Reduction of Thermal Stresses in Functionally Gradient Materials," Computer Methods in Applied Mechanics and Engrng., vol. 106, pp. 271-284, 1993.

[13] K. Tanaka, Y. Tanaka, H. Watanabe, V.F. Poterasu, Y. Sugano, "An Improved Solution to Thermo elastic Materials Designed in Functionally Gradient Materials: Scheme to Reduce Thermal Stresses," Computer Methods in Applied Mechanics and Engineering, vol. 106, pp. 377-389, 1993.

[14] G.R. Liu and Y.T. Gu, "A Point Interpolation Method for Two-Dimensional Solids," International Journal for Numerical Methods in Engineering, vol. 50, no. 4, pp. 937-951, 2001.

AUTHOR BIOGRAPHY

Dr. Lai received his Ph.D. degree from Mechanical Engineering Department in University of Wisconsin-Madison in 1984. He joined North Carolina A&T State (NCA&T) University as a full-time faculty member in the summer of 1984. Dr. Lai had served as the Director of NASA Center of Research Excellence during 1990-1993 in NCA&T. He became tenured in 1990 and received his full professorship in 1993 at NCA&T. After working in United States for ten years, Dr. Lai decided to go back to Taiwan to teach in his mother university, National Cheng- Kung University (NCKU). Dr. Lai is active in both academic and industrial sectors. Dr. Lai's research interests include mathematical modeling, micro-macro systems engineering, design of experiments, and universal exploration.

Jing-Hao Kang is a Ph.D. student in the Department of Mechanical Engineering at National Cheng-Kung University. He is currently working in the areas of micro pump system design and malfunction detection for modification and refinement.